ADVANCED MATERIALS
www.advmat.de

3D Printing of Micrometer-Sized Transparent Ceramics with On-Demand Optical-Gain Properties

Ido Cooperstein, S. R. K. Chaitanya Indukuri, Alisa Bouketov, Uriel Levy, and Shlomo Magdassi**

Transparent ceramics are usually polycrystalline materials, which are wildly used in many optical applications, such as lasers. As of today, the fabrication of transparent ceramic structures is still limited to conventional fabrication methods, which do not enable the formation of complex structures. A new approach for 3D printing of micrometer-size, transparent ceramic structures is presented. By using a solution of metal salts that can undergo a sol–gel process and photopolymerization by two-photon printing, micrometer-sized yttrium aluminum garnet (YAG) structures doped with neodymium (Nd) are fabricated. The resulting structures are not only transparent in the visible spectrum but can also emit light at 1064 nm due to the doping with Nd. By using solution-based precursors, without any particles, the sintering can be performed under air at ambient pressure and at a relatively low temperature, compared to conventional processes for YAG. The crystalline structure is imaged at atomic resolution by ultrahigh-resolution scanning transmission electron microscopy (STEM), indicating that the doped Nd atoms are located at the yttrium positions. Such miniaturized structures can be used for diverse applications, e.g., optical components in high-intensity laser systems, which require heat resistance, or as light sources in optical circuits.

Transparent ceramics are glassy or crystalline materials that are used in various applications such as optical fibers for guided light-wave transmission, optical switches, laser amplifiers and lenses, in the form of thin films, fibers, or 3D objects. These are inorganic materials composed of metal oxides, nitrides, fluorides, or sulfides that allow light to pass through at wavelengths ranging from deep-UV to near-IR.[1,2] While single-crystalline ceramics are usually defect free, the optical transparency of polycrystalline materials is limited since they are composed of numerous domains such as grains, grain boundaries, pores, and impurities, which usually cause light scattering.[2–5] On the other hand, in contrast to processes for the formation of single crystals, the fabrication of polycrystalline ceramics is much less time consuming, the materials possess better mechanical properties, and in principle can be made with complex 3D geometries. These advantages make polycrystalline ceramics very attractive for utilization in various optical applications (lenses, thermal sensors, scintillators, solar cells, electro-optics, lasers, on-chip light sources, photonic circuits, etc.).[6–13] However, most current fabrication methods of transparent ceramics are based on conventional processes, such as powder pressing[14] or gel casting,[15] that only enables formation of objects with simple geometries and therefore limits their potential use in advanced applications which require complex structures. Additive manufacturing, also known as 3D printing, is a technology that may enable overcoming this structural limitation.[16–21] To the best of our knowledge, there is only one publication reporting on 3D printing of transparent ceramics, by using a direct ink writing (DIW) process, at low resolution. Furthermore, in this research only simple 3D shapes (core–shell rods) were printed by using a slurry of ceramic particles, for which the sintering should be performed under very high pressure by costly instrument (high isostatic pressure, HIP).[22]

Advanced 3D printing technologies that are based on photopolymerization such as two-photon printing (TPP) and continuous liquid interphase printing (CLIP) opens the way to fabricate highly complex structures with printed features in the nano- and micrometer ranges, respectively.[23,24] In TPP, a high-power femtosecond laser beam with a wavelength of 780 nm is focused within a resin containing photoinitiator (PI) that adsorbs in the UV range. At the focal point, two photons are absorbed, and at this small voxel, these two photons excite the PI and cause a localized radical polymerization of the resin.[25] This approach requires the selection of suitable PI, the presence of photocurable groups in the resin (such as acrylates) and avoiding particles in the ink to avoid scattering. While there are various reports on achieving advanced optical properties affected by their geometries (such as variable refractive index[26]

I. Cooperstein, A. Bouketov, Prof. S. Magdassi
Casali Center for Applied Chemistry
Institute of Chemistry and Center for Nanoscience and Nanotechnology
The Hebrew University of Jerusalem
Jerusalem 91904, Israel
E-mail: magdassi@mail.huji.ac.il
Dr. S. R. K. C. Indukuri, Prof. U. Levy
Department of Applied Physics
Faculty of Science and the Center for Nanoscience and Nanotechnology
The Hebrew University of Jerusalem
Jerusalem 91904, Israel
E-mail: ulevy@mail.huji.ac.il
The ORCID identification number(s) for the author(s) of this article can be found under https://doi.org/10.1002/adma.202001675.

DOI: 10.1002/adma.202001675

or intensity distribution and shaping[27]), in these demonstrations only organic or hybrid organic–inorganic materials were used for printing. Such materials are limited for high-performance optical applications; for example, they cannot be used in applications that require high-power light sources due to the low damage threshold in contrary to transparent ceramics.[28] Therefore, there is a need to develop printing compositions for achieving transparent ceramic 3D objects. Several reports on printing ceramic structures were published in the recent years. Gailevičius et al.[29] reported on a glass-ceramic structure obtained by printing the commercial ink SZ2080 followed by burning it at elevated temperatures. The ink was hybrid organic–inorganic material with ≈43 wt% of silica and zirconia precursors. Upon heating up to 1200 °C, silica glass with mainly amorphous structure was formed, and upon further heating a mixture of SiO_2 (cristobalite) together with t-ZrO_2 was detected. Brigo et al.[30] reported on printing commercial hybrid ink containing silica backbones. By pyrolyzing the structure under inert gas at 1000 °C, the structure becomes SiOC, which has high thermal stability and high mechanical properties. Yee et al.[31] reported on obtaining functional ZnO structure with electromechanical properties by printing metal salt within organic monomer followed by heating under air. However, none of the above are transparent and therefore cannot be used for optical applications.

Here we present a new approach for 3D printing transparent multiatom polycrystalline objects by TPP process while using new ink compositions.

We demonstrate the new approach for fabricating 3D objects composed of polycrystalline transparent yttrium aluminum garnet (YAG, $Y_3Al_5O_{12}$) structures that are doped with rare-earth metals to make it capable of emitting light upon irradiation. YAG was chosen due to its wide use in many optical applications, e.g., acting as a lasing medium when doped with rare-earth metal elements, such as neodymium. Based on our previous reports on 3D printing of transparent silica glass,[32,33] we synthesized ink compositions without any particles, which are based on a sol–gel process of metal salts in the presence of acrylic acid. The ink was printed by TPP method, followed by heating the obtained micrometric structures to remove the organic material and to promote initiation and growth of the crystals. To the best of our knowledge only one publication demonstrated printing of complex YAG structure, but the resultant structure is not transparent and the ink contains particles and therefore cannot be printed by TPP.[34] The millimeters size YAG structures were fabricated by a digital light processing (DLP) printer, followed by heating to 1600 °C to obtain a dense structure.

Here we report on fabricating complex transparent YAG with nanometric resolution, which is photoluminescent when doped with neodymium, suggesting that the structure can act as a lasing medium. The approach based on a solution enables very simple doping process and performing the post printing heat process at a relatively low temperature, 1100 °C, compared to conventional processes for obtaining transparent polycrystalline YAG. It is expected that this approach will facilitate applications, which require optical elements with high damage thresholds and for fabricating on-chip light sources for high-speed optical communication systems. This currently is mainly done either by wafer bonding of a III–V layer into the chip,[35] or alternatively by using by CVD,[36] soft lithography[37] or by direct writing inside doped crystals.[38] The new approach will also open possibilities in the general field of fabrication of transparent polycrystalline ceramics composed of several metals.

The ceramic ink was prepared by combining photopolymerization with a sol–gel reaction of metal salts in aqueous solution (**Figure 1**a). Upon dissolution in water, the metal salts transform to hydroxides and the pH of the solution decreases. Addition of propylene oxide (PO) promotes the gelation by scavenging the protons in the solution and thus increases the pH.[39,40] To make the ink photopolymerizable, acrylic acid was added, which also forms coordination bonds with aluminum and yttrium ions. Ethylene glycol was also added to decrease the surface tension of the ink in order to prevent cracking of the printed objects, and a photoinitiator was added to initiate the radical polymerization upon the printing process. Since the printed structures require sintering at high temperature, the ink was printed on a sapphire base (melting point ≈2000 °C). The two-photon printing process was performed by localized photopolymerization within the ink droplet (Figure 1b), followed by washing in volatile solvent (Figure 1c) and removal of the organic material at high temperature (Figure 1d). Typical printed micrometer-size YAG structures after removal of all the organic material are presented in Figure 1e–g. After printing, the objects are composed of organic–inorganic network, and after heating to 620 °C the objects are composed of amorphous inorganic material. Further heating above 920 °C causes crystallization, and the resulting objects are polycrystalline YAG (as measured by XRD and presented in Figure S1, Supporting Information). It should be noted that the total concentrations of the precursors ($AlCl_3$ and YCl_3) are crucial for obtaining a single, homogenous phase. At high concentrations (49 wt%) the resulting structure is composed of two phases: a continuous alumina phase with dispersed of 0.2–1 μm YAG crystals (Figure S2, Supporting Information). Decreasing the concentration of the precursors leads to a gradual increase in the content of the YAG phase until only a single-phase YAG structure is obtained (at 25 wt% precursors).

To address an optical application such as lasing, by the transparent polycrystalline objects, the YAG should be doped with rare-earth metal.[41] Therefore, we dissolved in the printing composition a neodymium salt. A Nd-doped YAG miniature light-splitter was printed (**Figure 2**a), followed by heating to 1100 °C (Figure 2b) and 1500 °C (Figure 2c). As shown in Figure 2d, the beam splitter after heating is composed of sintered particles.

In order to evaluate the chemical composition and the crystalline structure of the printed objects, thin slices were cut by focused ion beam (FIB) from printed Nd:YAG plates, and characterized by element mapping at atomic resolution. As clearly seen, each particle is a single crystal, and its structure is in full agreement with the known Nd:YAG structure (PDF Card-04-017-6068) (Figure 2e,f taken at zone axis 100). Figure 2e shows the elemental mapping of the three elements, and Figure 2f (without the Al) shows that the Nd ions occupy mostly the yttrium places, as could be expected for replacement of ions having similar sizes.[42] Additional support for the specific crystalline structure is presented for more zone axes in Figure 2g. To examine the homogeneity of the crystals composing the

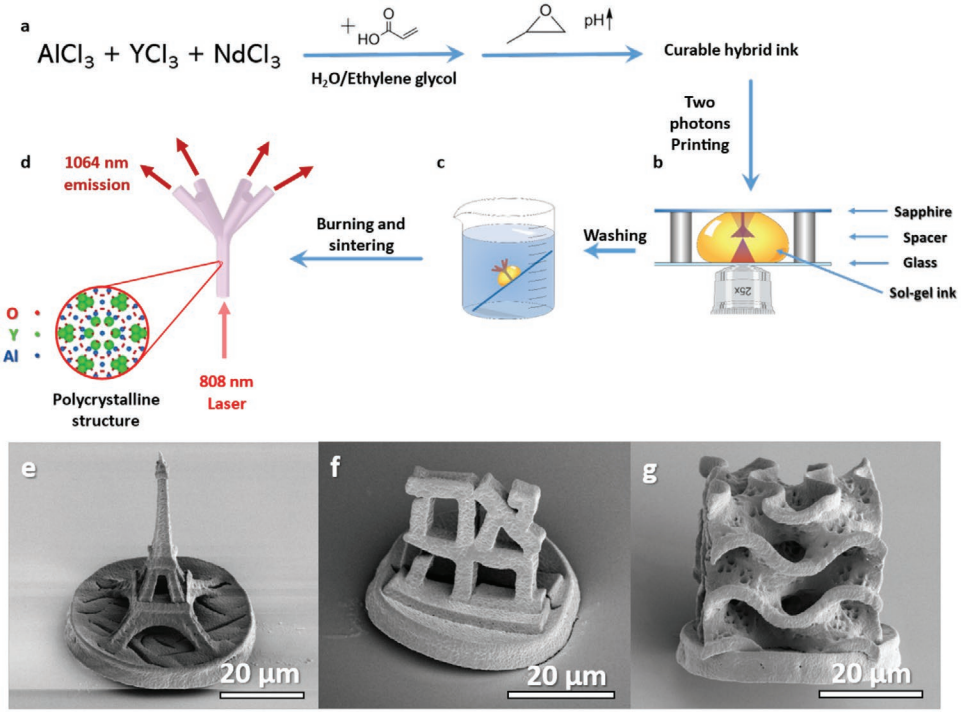

Figure 1. Scheme illustrating the preparation of doped YAG 3D structure. a) Starting from metal salts dissolved in water and ethylene glycol together with acrylic acid, followed by addition of PO at the second stage. b) At the next stage, printing of the ink using a two photon printer on top of a sapphire base was performed, c) followed by washing the obtained 3D object from uncured ink. d) Final heating at elevated temperature was performed to form single phase Nd:YAG. e–g) Printed polycrystalline structures after heating to 1500 °C.

structure, and their packing, TEM images of the entire cross-section of printed plates were taken. Figure S3a,b and c,d present cross-section of undoped and doped structures, respectively. As shown, after heating to 1500 °C the printed objects are dense and contain small number of holes or do not contain holes (as seen in the doped sample). Due to the small size of the object, it is composed of only one or two crystals along its height, allowing the light to go through without many diffraction sites. The elemental mapping shows that all the crystals are composed of the same percentage of yttrium and aluminum (Figure S3b, Supporting Information) or yttrium, aluminum, and neodymium (Figure S3c, Supporting Information), which are homogenously distributed within the single-phase crystals. EDS measurements (Figure S4, Supporting Information) testify the composition to be $Y_{3.3}Al_{5.1}O_{12}$ for undoped structures and $Y_{2.53}Nd_{0.09}Al_{5.88}O_{12}$ for Nd doped structures (3.4 at% from Y). These ratios are very close to the metal salts ratio in the printing composition, indicating the strength of the proposed solution-based approach for making polycrystalline structure with predesigned compositions.

It is important to note that there are some impurities in the object as can see in Figure S4 (Supporting Information), the origin of them is unknown and they were not inserted to the ink formulation, we suspect that they might be from the used oven.

In addition, in some of the experiments, we observed phase separation, resulting in structures composed of yttrium aluminum perovskite (YAP), as shown in Figure S5 (Supporting Information).

It should be noted that this approach is accompanied by high shrinkage: while one may consider it as a drawback, it can also be an advantage in obtaining feature sizes, which are smaller than the typical sizes of printed objects composed of organic monomers. Finer feature size due to shrinkage can be also obtained by changing the precursor's concentrations, as long as the crystalline phases do not change upon changes of precursor compositions. Overall, the shrinkage of the objects is about 68% compared to the CAD designed structures. The shrinkage is demonstrated in Figure 2: As printed objects are presented in Figure 2a, then heated objects to 1100 °C (Figure 2b) and final shrinkage at 1500 °C (Figure 2c). Shrinkage usually occurs due to gelation and crosslinking, due to the capillary forces that apply on the structure upon removal of materials[43] and by densification of the crystalline structure. In our system, the first shrinkage (32%) compared to the CAD file is due to by dehydration of the structures at room temperature. The thermal treatment was followed by TGA/DSC measurements (Figure S6, Supporting Information). As seen, upon heating to 200 °C there was a weight loss of 53%, due to evaporation of the remaining solvent. Further heating to 620 °C results in removal of the polymerized organic material, which led to additional weight loss of 28%. Heating to 920 °C initiates the crystallization of the structure (DSC measurements, Figure S6, Supporting Information) which results in densification of the obtained structure. The overall weight loss after heating to 1500 °C is 83 wt%, and the measured linear shrinkage is about 62%–68%. Furthermore, the shrinkage is isotropic and the structure does not deform due to the high shrinkage, as

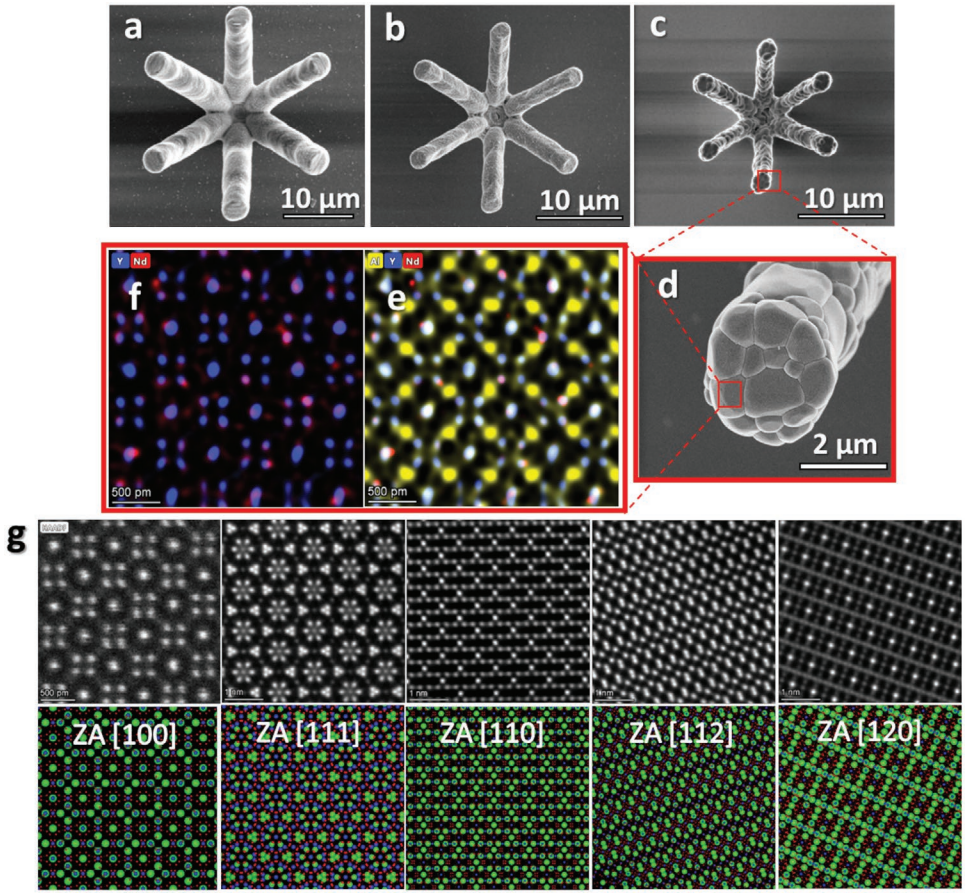

Figure 2. SEM and TEM images of printed Nd:YAG structures. a–c) Nd:YAG structure after different heating profiles: a) after printing, b) after heating to 1100 °C, c) after heating to 1500 °C. d) Higher magnification of (c). e,f) Ultrahigh magnification of one of the crystals comprising the Nd:YAG structure at zone axis 100: e) element image of Al, Y, and Nd, and f) element image of Y and Nd. g) TEM images of the atomic lattice at different zone axes. Theoretical simulations of each zone axis are displayed beneath each image.

can be seen in Figure S7 (Supporting Information). In addition, due to the high shrinkage, the structures can deform and sometimes suffers from cracks, as can be seen on the rafts of Figure 1e,f (the pores in Figure 1g are predesigned features). The cracks and deformation occur during sintering and can be avoided by the design of structure, and mainly by printing suitable supports (such as those that were printed and presented in Figure 1e,g)[30,44] Moreover, due to the crystallization process, the surface becomes rough, as can be seen in Figure 2d. This roughness can reduce the efficiency of optical application. To overcome this problem, a chemical polishing may smooth the surface by immersing the structure into hot phosphoric acid.[38,45]

Furthermore, the printing compositions yield objects with high thermal stability. As can be observed in Figure S6 (Supporting Information), there is no mass loss between the crystallization point at 920 °C and the final heating stage at 1500 °C (less than 2 wt%). This lack of mass loss indicates thermal stability of the structures to at least 1500 °C.

To demonstrate transparency, Nd-doped YAG plates were printed with a thickness of about 1.5 µm on top of a printed image "HUJI" which is located beneath the plates. After heating, the plate shrinks (opposite to the HUJI letters) and reveal the letters "H" and "I" while still covering the letters "UJ" that can only be seen by optical microscopy if the plate is transparent to visible light. After heating to the crystallization temperature (920 °C), the plate is highly transparent (**Figure 3**a). At this stage, the crystals were very small, with average size of 50.5 nm (evaluated by SEM imaging, Figure 3e), and there is negligible scattering of visible light. After heating to 1100 °C (Figure 3b), the crystal size grows to about 94 ± 25 nm (evaluated by SEM imaging Figure 3f), and the structure is still transparent. After heating to 1250 °C (Figure 3c), the crystal size grows to about 289 nm (evaluated by SEM imaging Figure 3g) and the structure is still transparent, even though the grains are noticeable. Only after heating to 1500 °C (Figure 3d), the crystals grow to sizes that cause diffraction of the visible light (≈750 nm, Figure 3h), and therefore the structure becomes translucent. Figure S8 (Supporting Information) shows the transparency calculated by spectral integrated transmission from optical images, indicating that the transparency decreases with temperature, starting from 98% in structures heated to 920 °C and decreasing to 70% for samples heated at 1500 °C. SEM images of the printed plates are presented in Figure S9a–d (Supporting Information). Due to the short distance between the letters and the plate, another structure with

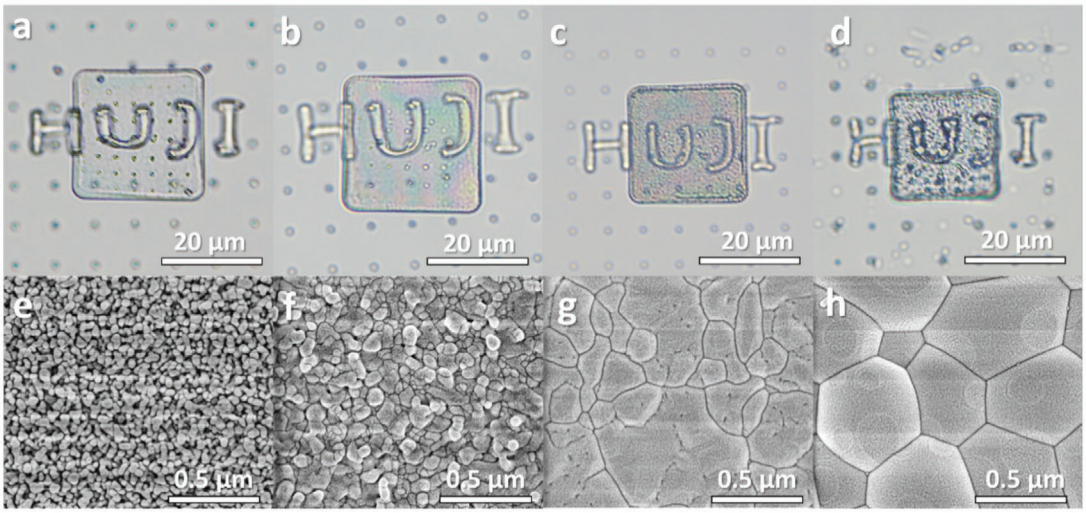

Figure 3. Optical and SEM images of printed Nd doped YAG plates with "HUJI" underneath heated to different temperatures. a–d) Optical images from above the plates: a) 920 °C, b) 1100 °C, c) 1250 °C, d) 1500 °C. e–h) SEM images of the plates surface, e) 920 °C, f) 1100 °C, g) 1250 °C, h) 1500 °C.

larger distance (28 µm before shrinkage) was printed and presented in Figure S9e–h, Supporting Information showing the same trend. In addition, it should be noted that below 1500 °C, the structure is porous (Figure S10, Supporting Information), and therefore, in order to close the pores and to reach higher density, the temperature was increased up to 1500 °C.

To examine the ability of the printed doped structures to act as a laser, we measured and took visual images of the light emission from the structures while irradiating them with a 785 nm laser. **Figure 4**a presents the measured emission from printed plates after various heat treatments. As seen, the strongest emission (typical for Nd:YAG at 1064 nm) is obtained from structures heated to 1500 °C compared to structures heated to 1250 °C, 1100 °C, and 920 °C, probably due to scattering from the pores and quenching by vibrational losses due to hydroxide groups that might be present on the surface.[46] The images of the IR emission were taken for light splitters having six branches, where the structure was irradiated from

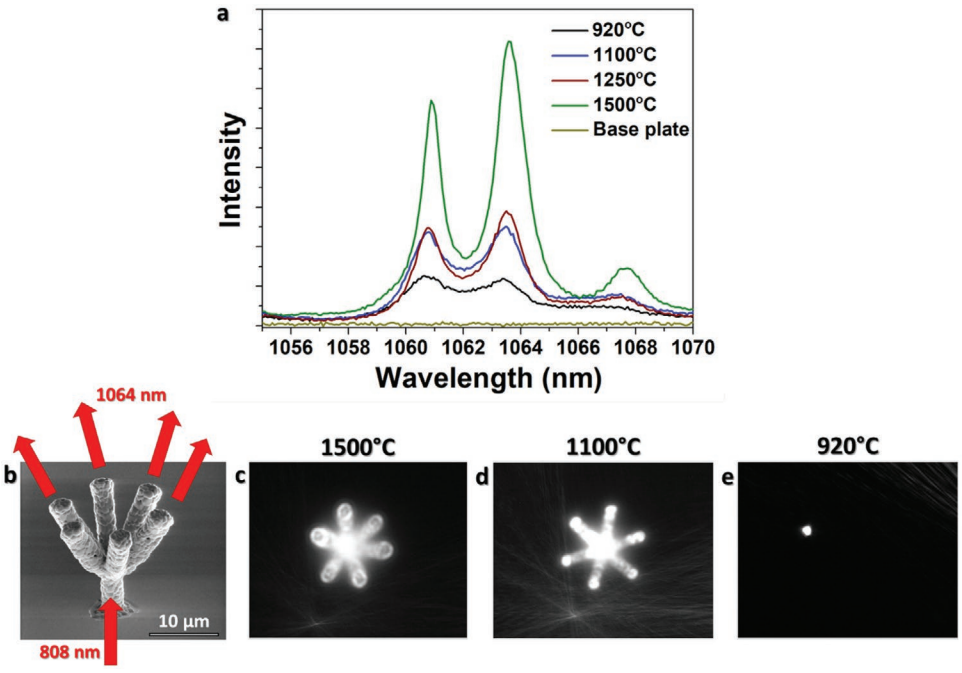

Figure 4. Emission spectra and optical imaging from printed Nd:YAG. a) Emission spectra of printed plate structures illuminated with 785 nm laser. b) SEM image of printed light splitter after heating to 1500 °C, the illustration describe the excitation of the structure by a laser at 808 nm wavelength from the bottom, and the emission from the structure at a wavelength of 1064 nm as seen from the optical images. c–e) The optical images taken from the top of the printed light splitter heated to different temperatures while laser hits in the middle of the structure: c) heated to 1500 °C; d) heated to 1100 °C; e) heated to 920 °C.

its bottom at a wavelength of 808 nm (Figure 4b). As seen, while being irradiated at the bottom of the structure, the laser splits into the six branches of the structure and IR light emits from them. As seen, emission is achieved only from structures heated above 1100 °C (Figure 4c,d) and not from the structures heated to 920 °C (Figure 4e). As was mentioned above, this is probably due to scattering from the pores and absorption by the hydroxide groups that are still present at 920 °C. Nevertheless, the emission from structures heated to 1100 °C means that an optical active transparent polycrystalline structure can be achieved at relatively low temperature without being fully dense. Such structure can be only achieved by fabricating a 3D structure from a sol–gel ink composition compare to inks containing particles that require high-temperature sintering.

Due to the visual light leakage at 808 nm even while using two filters of 850 and 900 nm, we have also taken a video with low resolution IR camera that cuts almost completely the 808 nm light (Video S1, Supporting Information). As shown, only when the laser hits the sample, the IR emission can be seen as a bright light emitted from the sample.

It should be noted that in the PL imaging measurement, we exposed the 3D structure to maximum laser power densities of 1.87 J cm^{-2} over few minutes and we neither see any change in the PL signal nor any material damage (no changes in the optical images). While the value of 1.87 J cm^{-2} is limited by our Ti-sapphire laser and the optical system transmission, we believe that the actual damage threshold is significantly higher. It should also be mentioned that this value is significantly higher than the value of 0.169 J cm^{-2} reported by of Butkutė et al. for structures printed from the commercial SZ2080 photoresin.[28]

In conclusion, TPP curable sol–gel printing compositions were developed for 3D printing of transparent polycrystalline micrometer-sized ceramic structures and demonstrated for fabrication of miniature YAG and Nd-doped YAG objects. The ink compositions enable doping by simply dissolving salts of the dopant within the ink compositions. The YAG structures show high transparency while heated below 1100 °C, and the Nd-doped YAG shows IR emission. The main emission is at 1064 nm, similar to the reported emission of commercial Nd:YAG lasers. Above 1100 °C, the structure becomes dense at 1500 °C, the emission increases, but the transparency decreases. In addition, by controlling the Al and Y precursor amount at the preparation step, nanocomposite of Al_2O_3/YAG can be made as well. Furthermore, due to the feasibility and versatility of the proposed approach, more polycrystalline objects can be easily formed. Samples of printed ruby (Cr:Al_2O_3) and yttrium oxide (YO_2) are presented in Figure S11 (Supporting Information). We expect that combining light induced polymerization and sol–gel processes performed in solutions, without using preformed particles, will open the way for utilization of polycrystalline ceramic structures as optical components providing high lighting power and high mechanical and thermal stability, as well as making devices with high damage threshold. This damage, such as in high-power lasers, is thermal, and originates from the irradiated light, which is absorbed by the sample. In addition, due to their emission properties, these objects can also be applied for micrometer-size lasers and as light sources for photonic systems. Examples are the integration of such light sources in chip-scale photonic communication systems at the intra chip and the inter chip level with applications in high-speed photonic circuitry for computers and data centers. Other examples include interfacing the demonstrated technology with plasmonic structures for enhancing light–matter interactions or the integration of the gain medium with metasurfaces for controlling the emission properties.

Experimental Section

Materials: Aluminum chloride hexahydrate ($AlCl_3{\cdot}6H_2O$) was purchased from Alpha Aesar (USA). Yttrium chloride hexahydrate ($YCl_3{\cdot}6H_2O$) and neodymium chloride hexahydrate ($NdCl_3{\cdot}6H_2O$) were purchased from Strem Chemicals (USA). Ethylene glycol, propylene oxide (PO), and Novec 7100 were purchased from Sigma Aldrich (USA). Photoinitiators 2-benzyl-2-dimethylamino-1-(4-morpholinophenyl)-butanone-1 (IRG 369) and diphenyl(2,4,6-trimethylbenzoyl) phosphine oxide (TPO) were kindly given by IGM Resins (The Netherlands). Sapphire lenses were purchased from Gavish Company (Israel).

Curable Ceramic Ink: YAG ink was prepared at room temperature by dissolving 11.4 wt% of $YCl_3{\cdot}6H_2O$ in 42.3 wt% of triple distilled water (TDW) and ethylene glycol (65% ethylene glycol in TDW). After 5 min of stirring, 13.9% of $AlCl_3{\cdot}6H_2O$ was added, and the mixture was stirred for 30 min. Then 4.2 wt% of acrylic acid was added and stirring was continued. After 30 min, 28.2 wt% of propylene oxide was added stepwise (half of the amount while stirring, and then the second half 1 min later). After stirring for 40 min, the photoinitiator IRG 369 was added at concentration of 0.75 wt%, and the mixture was stirred until complete dissolving of the components. For formulating the doped YAG with neodymium, $NdCl_3{\cdot}6H_2O$ was added 5 min after the addition of $AlCl_3{\cdot}6H_2O$ at the desirable doping amount. The formulations were mixed with a magnetic stirrer (model MR Hei-Tec, Thermo Fisher) at the maximal stirring rate of 1400 rpm.

Two-Photon Printing: The printing was done using a Photonic Professional GT printer (Nanoscribe GmbH, Germany). The ink was placed between glass and sapphire lens with a custom-made metal spacer between them at height of 140 µm as can be seen in Figure 1b. The printing was performed with a ×25 magnification lens. After printing, the sapphire base with the printed structure was washed by immersing it in ethanol for 5 min while stirring and then in Novec 7100 for 1 min for quick drying after exposing the structure to air.

Heating Profile: After the printing, the structure was heated under air at tube oven (Zhengzhou Kejia Furnace, China) to different temperatures: 200 °C and dwelling time of 2 h, then to 520 °C with dwelling time of 2 h, and finally to 620 °C with dwelling time of 5 h (all heating rates were rate of 0.6 °C min^{-1}). Then the obtained structures undergone further heating under air at the required temperatures, 920 °C, 1100 °C, 1250 °C or 1500 °C at dwelling time of 5 h.

Characterization: Electron Microscopy: Scanning electron microscopy (SEM) imaging was done with Magellan 400L (FEI company, USA). High-resolution scanning transmission electron microscopy (STEM) imaging was done with probe corrected scanning transmission electron microscope themis-Z operated at 300 KV and equipped with SuperX EDS detector (Thermo Fisher Scientific, USA). STEM samples and cross section cuts were prepared by using a focused ion beam scanning electron microscope (FIB, FEI Company, USA).

Thermal analyses were performed by using simultaneous thermogravimetry (TGA)–differential scanning calorimetry (DSC) manufactured by NETZSCH-Geratebau GmbH. The measurements were done at a heating rate of 5 °C to 1500 °C under air.

Characterization: Structure and Material Analysis: X-ray diffraction (XRD) measurement was done with Smartlab SE (Rigaku, Japan).

Characterization: Optical Characterization: Photoluminescence (PL) measurements were performed with the use of inVia confocal Raman microscope (Renishaw, UK) equipped with a 785 nm diode laser with power of 300 mW. The measurements were done by irradiating printed

plate samples at power of 5×10^{-6} % and the PL was collected by CCD detector. The presented data were based on an average of four samples that were heated to 1100 °C, 1250 °C, and 1500 °C, and average of three samples of structures heated to 920 °C. Optical images (Figure 3) were taken with upright optical microscope BX53M (Olympus, Japan) by using ×100 lens, and lighting the structures from below. Due to very small size of the 3D printing area, conventional transmission measurements are not possible in our system. Optical images taken in transmission mode to estimate the transmission were used. This is possible due to each optical image contains both 3D printed plate and surrounding substrate in the same illumination area. All the images were saved in true color (RGB) format and by using MATLAB code the RGB values of each pixel were analyzed. For obtaining the spectral integrated transmission measurements (Figure S8, Supporting Information), the ratio of the total value of RGB was taken for each pixel inside the 3D printed area and outside the 3D printing area. Up to 12 pixels were performed from each region to achieve mean value of transmission. Mean of the statistical distribution of transmission was taken as error bar in the graph.

Characterization: Photoluminescence Optical Imaging: PL imaging measurements were performed using a modified inverted microscope (Nikon) in transmission mode as shown in the schematic diagram (Figure S12, Supporting Information). For excitation, Ti-sapphire (Tsunami) laser with 808 nm and 100 fs pulses with 80 MHz reputation rate was focused on to the sample with 50× objective. Emission PL signal collected with both 50× and 100× objectives (air) on top illumination system and focused on to the IR Camera (InGaAs Camera). Same objects were used from sample imaging with white light illumination microscopy with a white light source (tungsten–halogen lamp). Two long pass filters 850 and 900 nm (Thorlab) were used to remove excitation signal from the PL in the imaging.

Supporting Information

Supporting Information is available from the Wiley Online Library or from the author.

Acknowledgements

This research was partially supported by grants from the Israel Ministry of Science and Technology, and the National Research Foundation, Prime Minister's Office, Singapore under its Campus of Research Excellence and Technological Enterprise (CREATE) program. The authors thank the Brodje lab at the Hebrew University for their printing services and support. Also, the authors thank the Nanocenter at the Hebrew University, with special thanks to Atzmon Vakahi for the FIB samples, and Dr. Sergei Remennik for the TEM images and analysis.

Conflict of Interest

The authors declare no conflict of interest.

Keywords

additive manufacturing, gain media, sol–gel processing, transparent ceramics, yttrium aluminum garnet

Received: March 9, 2020
Revised: April 2, 2020
Published online: May 17, 2020

[1] S. F. Wang, J. Zhang, D. W. Luo, F. Gu, D. Y. Tang, Z. L. Dong, G. E. B. Tan, W. X. Que, T. S. Zhang, S. Li, L. B. Kong, *Prog. Solid State Chem.* **2013**, *41*, 20.
[2] Z. Xiao, S. Yu, Y. Li, S. Ruan, L. B. Kong, Q. Huang, Z. Huang, K. Zhou, H. Su, Z. Yao, W. Que, Y. Liu, T. Zhang, J. Wang, P. Liu, D. Shen, M. Allix, J. Zhang, D. Tang, *Mater. Sci. Eng., R* **2020**, *139*, 100518.
[3] U. Anselmi-Tamburini, J. N. Woolman, Z. A. Munir, *Adv. Funct. Mater.* **2007**, *17*, 3267.
[4] J. Petit, P. Dethare, A. Sergent, R. Marino, M.-H. Ritti, S. Landais, J.-L. Lunel, S. Trombert, *J. Eur. Ceram. Soc.* **2011**, *31*, 1957.
[5] G. C. Wei, *J. Phys. D: Appl. Phys.* **2005**, *38*, 3057.
[6] S. Noda, A. Chutinan, M. Imada, *Nature* **2000**, *407*, 608.
[7] C. Yeh, F. Shimabukuro, P. Stanton, V. Jamnejad, W. Imbriale, F. Manshadi, *Nature* **2000**, *404*, 584.
[8] U. Peuchert, Y. Okano, Y. Menke, S. Reichel, A. Ikesue, *J. Eur. Ceram. Soc.* **2009**, *29*, 283.
[9] A. S. S. de Camargo, J. F. Possatto, L. A. D. O. Nunes, É. R. Botero, É. R. M. Andreeta, D. Garcia, J. A. Eiras, *Solid State Commun.* **2006**, *137*, 1.
[10] C. Xiong, W. H. P. Pernice, H. X. Tang, *Nano Lett.* **2012**, *12*, 3562.
[11] T. Yanagida, H. Takahashi, T. Ito, D. Kasama, T. Enoto, M. Sato, S. Hirakuri, M. Kokubun, K. Makishima, T. Yanagitani, H. Yagi, T. Shigeta, T. Ito, *IEEE Trans. Nucl. Sci.* **2005**, *52*, 1836.
[12] J. You, L. Meng, T. Bin Song, T. F. Guo, W. H. Chang, Z. Hong, H. Chen, H. Zhou, Q. Chen, Y. Liu, N. De Marco, Y. Yang, *Nat. Nanotechnol.* **2016**, *11*, 75.
[13] T. Taira, *Opt. Mater. Express* **2011**, *1*, 1040.
[14] L. Ge, J. Li, Z. Zhou, B. Liu, T. Xie, J. Liu, H. Kou, Y. Shi, Y. Pan, J. Guo, *Opt. Mater.* **2015**, *50*, 25.
[15] X. Qin, G. Zhou, Y. Yang, J. Zhang, X. Shu, S. Shimai, S. Wang, *Ceram. Int.* **2014**, *40*, 12745.
[16] M. Zarek, M. Layani, I. Cooperstein, E. Sachyani, D. Cohn, S. Magdassi, *Adv. Mater.* **2016**, *28*, 4449.
[17] D. K. Patel, A. H. Sakhaei, M. Layani, B. Zhang, Q. Ge, S. Magdassi, *Adv. Mater.* **2017**, *29*, 1606000.
[18] T. Rosental, S. Magdassi, *Adv. Eng. Mater.* **2019**, *21*, 1900604.
[19] D. Kam, M. Layani, S. BarkaiMinerbi, D. Orbaum, S. Abrahami BenHarush, O. Shoseyov, S. Magdassi, *Adv. Mater. Technol.* **2019**, *4*, 1900158.
[20] N. Guo, M. C. Leu, *Front. Mech. Eng.* **2013**, *8*, 215.
[21] R. L. Truby, J. A. Lewis, *Nature* **2016**, *540*, 371.
[22] I. K. Jones, Z. M. Seeley, N. J. Cherepy, E. B. Duoss, S. A. Payne, *Opt. Mater.* **2018**, *75*, 19.
[23] S. Kawata, H. B. Sun, T. Tanaka, K. Takada, *Nature* **2001**, *412*, 697.
[24] J. R. Tumbleston, D. Shirvanyants, N. Ermoshkin, R. Januszewicz, A. R. Johnson, D. Kelly, K. Chen, R. Pinschmidt, J. P. Rolland, A. Ermoshkin, E. T. Samulski, J. M. DeSimone, *Science* **2015**, *347*, 1349.
[25] Q. Geng, D. Wang, P. Chen, S.-C. Chen, *Nat. Commun.* **2019**, *10*, 2179.
[26] F. Zhou, W. Cao, B. Dong, T. Reissman, W. Zhang, C. Sun, *Adv. Opt. Mater.* **2016**, *4*, 1034.
[27] T. Gissibl, S. Thiele, A. Herkommer, H. Giessen, *Nat. Commun.* **2016**, *7*, 11763.
[28] A. Butkutė, L. Čkanavičius, G. Rimšelis, D. Gailevičius, V. Mizeikis, A. Melninkaitis, T. Baldacchini, L. Jonušauskas, M. Malinauskas, *Opt. Lett.* **2020**, *45*, 13.
[29] D. Gailevičius, V. Padolskytė, L. Mikoliūnaitė, S. Šakirzanovas, S. Juodkazis, M. Malinauskas, *Nanoscale Horiz.* **2019**, *4*, 647.
[30] L. Brigo, J. E. M. Schmidt, A. Gandin, N. Michieli, P. Colombo, G. Brusatin, *Adv. Sci.* **2018**, *5*, 1800937.
[31] D. W. Yee, M. L. Lifson, B. W. Edwards, J. R. Greer, *Adv. Mater.* **2019**, *31*, 1901345.

[32] I. Cooperstein, E. Shukrun, O. Press, A. Kamyshny, S. Magdassi, *ACS Appl. Mater. Interfaces* **2018**, *10*, 18879.
[33] E. Shukrun, I. Cooperstein, S. Magdassi, *Adv. Sci.* **2018**, *5*, 1800061.
[34] G. A. Dosovitskiy, P. V Karpyuk, P. V Evdokimov, D. E. Kuznetsova, V. A. Mechinsky, A. E. Borisevich, A. A. Fedorov, V. I. Putlayev, A. E. Dosovitskiy, M. V Korjik, *CrystEngComm* **2017**, *19*, 4260.
[35] D. Liang, J. E. Bowers, *Nat. Photonics* **2010**, *4*, 511.
[36] J. Liu, P. D. Garcia, S. Ek, N. Gregersen, T. Suhr, M. Schubert, J. Mørk, S. Stobbe, P. Lodahl, *Nat. Nanotechnol.* **2014**, *9*, 285.
[37] W. J. Lee, H. Kim, J. B. You, D. L. Huffaker, *Sci. Rep.* **2017**, *7*, 9543.
[38] A. Ródenas, M. Gu, G. Corrielli, P. Paiè, S. John, A. K. Kar, R. Osellame, *Nat. Photonics* **2019**, *13*, 105.
[39] X. Guo, W. Li, K. Nakanishi, K. Kanamori, Y. Zhu, H. Yang, *J. Eur. Ceram. Soc.* **2013**, *33*, 1967.
[40] Y. Tokudome, K. Fujita, K. Nakanishi, K. Kanamori, K. Miura, K. Hirao, T. Hanada, *J. Ceram. Soc. Jpn.* **2007**, *115*, 925.
[41] N. P. Barnes, B. M. Walsh, *IEEE J. Quantum Electron.* **1999**, *35*, 101.
[42] E. Kanchanavaleerat, D. Cochet-Muchy, M. Kokta, J. Stone-Sundberg, P. Sarkies, J. Sarkies, J. Sarkies, *Opt. Mater.* **2004**, *26*, 337.
[43] K. Kajihara, *J. Asian Ceram. Soc.* **2013**, *1*, 121.
[44] T. W. Lim, Y. Son, D.-Y. Yang, T. A. Pham, D.-P. Kim, B.-I. Yang, K.-S. Lee, S. H. Park, *Int. J. Appl. Ceram. Technol.* **2008**, *5*, 258.
[45] J. Basterfield, *J. Phys. D: Appl. Phys.* **1969**, *2*, 1159.
[46] M. Pokhrel, N. Ray, G. A. Kumar, D. K. Sardar, *Opt. Mater. Express* **2012**, *2*, 235.